Breast cancer development at the fat-gland interface (FGI): Importance of coronal imaging and ultrasound tomography.

[1-4]Peter J. Littrup, M.D., [2,3]Nebojsa Duric, PhD, [3]Mark Sak, PhD, and Rachel Brem, M.D.[4]

Prof. of [1]Radiology and [2]Oncology, Wayne State University, Detroit, Michigan, USA. Co-founder and Medical Advisor, [3]Delphinus Medical Technologies, Inc., Novi, Michigan, USA. [4]George Washington University

*E-mail: plittrup@delphinusmt.com

Abstract

Objective: We evaluated the locations of cancer and benign masses in relation to the fat-gland interface and anatomic quadrant locations with ultrasound tomography.

Methods: A total of 602 breast masses were evaluated from a clinical data set corresponding to a pre-trial arm of a multicenter study evaluating UST. Anatomic breast quadrants also noted for each tumor, and the fat-gland interface was considered the site of origin if at least 1/8 of the mass circumference abutted fat. In a subset of 298 masses, a hand-traced region-of-interest allowed quantitative sound speed and percent density comparisons of tumor and peritumoral margins.

Results: Cancers were located at the fat-gland interface in 93.4 % (169/181) of cases, and were completely surrounded by fat in 5.5% (10/181) or parenchyma in 1.1 % (2/21)($p<0.001$) of cases. Moreover, 56.1% (97/173) of cysts and 25.0% (47/188) of fibroadenomas were fully surrounded by dense tissue, significantly more than cancers (1.1%)($p<0.001$). The upper outer quadrant was the most common location of all masses, but no significant differences between mass were noted ($p=0.06$). Quantitative sound speed values showed significantly greater amount of fat surrounding cancers than fibroadenomas or cysts ($p<0.001$), while percent density showed that most cysts were completely surrounded by dense tissue and cancers were surrounded by both dense and fatty tissues.

Conclusion: Both the qualitative tumor location and quantitative peritumoral data corroborate the preferential location of cancers at the FGI, compared to benign masses or anatomic quadrants. This study supports possible integration into clinical practice with future dense breast screening by UST.

Keywords: breast cancer, fat-glandular interface, ultrasound tomography

1 Introduction

1.1 Breast Imaging and the Fat-Glandular Interface (FGI)

Imaging of breast cancer development is limited to macroscopic findings (e.g., >5 mm) by each modality. 3D localizations of cancer origin according the dominant breast tissues of denser fibroglandular parenchyma or fat are not commonly considered. Common mammographic teaching has emphasize greater visual attention to anatomic regions of historically higher cancer incidence (1,2), such as the upper outer quadrants having its greater parenchymal content, or epithelial distribution (2). The dominant signs of breast cancer by mammography relate to a focal mass/asymmetry, a cluster of microcalcifications and/or architectural distortion.

Cancers newly diagnosed by mammography were seen as a mass/asymmetry in over 2/3 of cases, by calcifications in 29% and architectural distortion in only 4% (3). Masses or asymmetries seen by mammography are generally then evaluated by ultrasound, which predominantly characterizes it as a cyst or solid mass for follow-up or biopsy, respectively. Yet, in women with overall increased breast density, mammography can miss up to 50% of cancers in the densest breasts and obscure both high contrast microcalcifications, as well as the higher density of some cancers.

Breast magnetic resonance (MR) imaging shows high sensitivity to both ductal carcinoma in situ (DCIS) and invasive cancers due to increased local blood flow and/or permeability to paramagnetic intravenous contrast agents. Limited breast MR work has suggested that the fat-glandular interface (FGI; figure 1) represents a preferable location for up to 94-99% of breast cancers (4,5). Breast cancer localization at the FGI appears to be a high sensitivity parameter but has not been widely considered. The coronal plane can visualize the circumferential nature of the FGI, which is feasible with 3D acquisitions of breast MR with isotropic pixels, but was not addressed (4,5). They also described benign solid masses, but cysts, the most common benign masses, were not included. In most women, fat makes up more of the

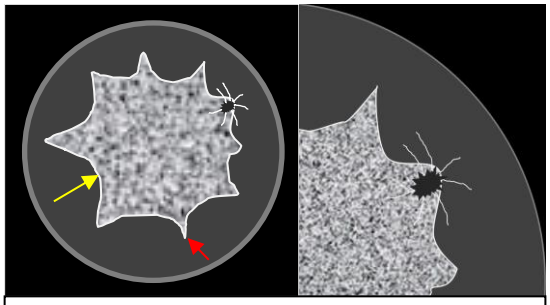

Figure 1: Graphic coronal representations of a UST sound speed (SS) image, highlighting the FGI (yellow arrow): The significantly higher SS of central fibroglandular tissue (speckled) allows good separation from the surrounding fat (darker gray). Red arrow denotes a Cooper's peak. Magnified view (right) shows an irregular cancer (black) at a Cooper's peak with radiating spicules of architectural distortion (white lines).

breast than dense tissue, which often leaves part of that coronal circumference without parenchyma, leaving only telltale residual fibrous bands (e.g., Cooper‘s ligaments) after involution.

1.2 The Well-Established Cancer Biology at the FGI

Breast cancer initiation and growth have strong associations with adjacent fat cells, or adipocytes, and their fat-secreted hormones, adipokines (6-7). The FGI also helps define the boundary with the breast‘s subcutaneous adipose layer which may comprise the largest endocrine gland in the body (8). Adipokines help mediate blood pressure, reproductive function, appetite, glucose homeostasis, angiogenesis and immune function (8). The link between obesity and the rising incidence of multiple diseases appears to include breast cancer.

When the balance of adipokines tip toward an excessive pro-inflammatory state at the FGI, multiple adipokines, such as leptin, have been implicated in breast cancer initiation via aromatase expression (9-10). Cancer cell lines and tumor growth become markedly accelerated in the presence of adipocytes (9). Bidirectional crosstalk between cancer cells and adipocytes, moreover lead to the formation of cancer-associated adipocytes (CAA). These CAA‘s stimulate a phenotypic change to generate fibroblast-like cells known as adipocyte-derived fibroblasts through the secretion of the adipokine, fibronectin, and collagen. Tumor cells cultured with these fibroblasts then demonstrate increased invasive ability. CAA‘s also display overexpression of collagen VI while ECM-related molecules contribute to breast cancer progression. This FGI sequence may also lead to the presence of a dense collagenous stroma, or desmoplastic reaction around breast cancers (i.e., peritumoral region), particularly in estrogen receptor/progesterone receptor (ER/PR) positive tumors.

1.3 UST and the FGI

Ultrasound tomography (UST) development over 40 years (11-36) has accelerated with recent rapid progress of computing capacity and appears well-suited to evaluate the circumferential nature of the FGI in its native coronal plane. A ring array transducer has provided whole breast and focal mass evaluation by combining reflection signal acquisition with quantitative transmission properties of sound speed (SS) and attenuation (ATT). UST offers quantitative multi-parametric evaluation of breast tissues that are scanned and displayed in its highest resolution, coronal plane. Correlation of mammographic breast density to SS distributions of parenchymal tissues throughout the breast have been thoroughly explored (26-36), including improvements in SS resolution (34). The excellent SS contrast between low SS fat and denser parenchyma/stromal tissues produced even better correlation with MR parenchymal patterns, as well as the volumetric assessment of the entire breast (37). SS has also been shown to be a stronger BC risk factor than mammographic density (32).

Given the strong biological background for cancer initiation near the FGI, we sought to clarify tissue localization for cancers, solid benign masses and cysts, in relation to their standard anatomic quadrants and tissue components using UST and its innate coronal imaging plane. In a smaller subset, mass evaluations by UST was also able to compare and assess quantitative peritumoral measurements.

2 Methods

For qualitative anatomic and FGI locations, a total of 602 clinical breast masses were noted within 467 individual breasts from 408 patients, as part of a related study of UST for women with dense breasts (SoftVue, Delphinus Medical Technologies Inc., Novi, Michigan; Clinicaltrials.gov – NCT#02977247). This data set included a subset with quantitative region-of-interest (ROI) analyses for the tumor and peri-tumoral regions noted below. Some women had more than one mass in each or both breasts. All masses were biopsy-confirmed by subsequent or prior histology, unless considered as a characteristic cyst by standard HHUS evaluation.

Mass location in coronal UST images was determined by a MQSA certified radiologist with extensive UST imaging experience. The relationship of a mass to the FGI was noted for a all 602 breast masses (181 cancers, 188 fibroadenomas, 173 cysts and 60 other benign findings), confirmed by biopsy, or by hand-held ultrasound for a simple cyst. The 60 other benign findings were excluded from the figures due to their smaller numbers and contained non-mass findings, such as focal fibrosis, micro-cystic changes and/or granulomatous mastitis.

The FGI was defined as the circumferential interface between the peripheral fat and parenchyma (4,5) as determined by examining sound speed (SS) images, which reliably differentiate the much lower SS (i.e., density) of fat (26-36) from the higher SS of fibroglandular tissues. Mass location was determined from its best visualized coronal level and placed into 3 groups: (i) completely surrounded by dense high SS fibroglandular tissue, (ii) completely surrounded by low SS fat or (iii) partially surrounded by both (i.e., the FGI) (4). Typically, if a mass showed ~1/8 of its circumference abutting fat in its greatest visualized coronal level, it was considered to be at the FGI (figure 2-Fibroadenoma). Conversely, a mass could be considered to abut parenchyma while being surrounded by fat and also labeled at the FGI (figure 2-Cancers). Masses were evaluated only on the coronal plane and therefore not fully evaluated in 3D for FGI location at this time due to lower out of plane resolution of SoftVue imaging (below). Mass location was only augmented by the lower resolution reconstructions in the axial/sagittal reconstructions as needed for additional confirmation of anterior/posterior aspects of the FGI. Masses were also categorized according to standard quadrant positions within the breast based on distance from the nipple and clock position of the finding. Differences in lesion locations were assessed using the chi-squared test.

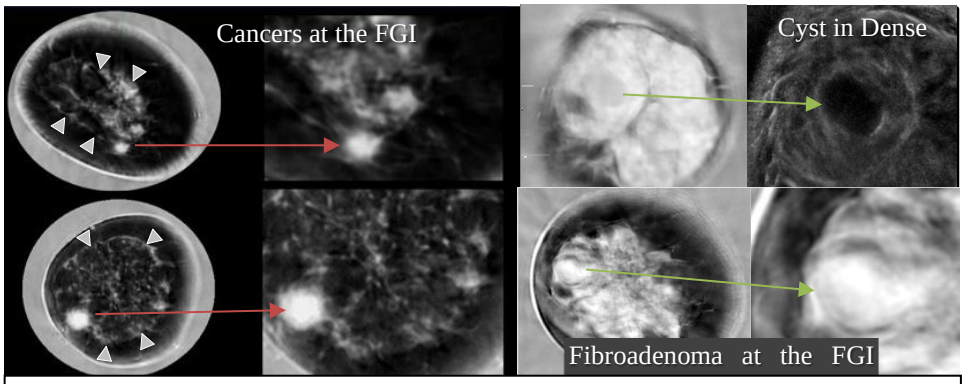

Figure 1 - ***Cancers, cyst and fibroadenoma:*** (Left) Sound speed (SS) images from 2 patients with scattered fibroglandular breast density and high SS cancers at the FGI. Both cancers have irregular margins on the magnified views, being nearly surrounded by fat along the residual fibrous bands of the FGI (arrowheads). Top right SS and magnified reflection view show dominant replacement by extremely dense breast parenchyma (white) with an embedded simple cyst. The well circumscribed 2.0 x 1.3 cm simple cyst has intermediate sound speed, similar to the gray water surrounding the breast. Bottom right images show a patient with heterogeneously dense breast parenchyma and a 1.6 x 1.2 cm fibroadenoma with a lucent halo of lower SS, sometimes also noted with mammography. While mostly embedded in parenchymal tissue, a smooth portion of the fibroadenoma bulges the FGI into the surrounding subcutaneous fat.

For a subset of 296 masses (78 cancers, 105 fibroadenomas, 91 cysts and 24 other benign findings), their boundaries were hand-traced by a radiologist with over 20 years experience as a certified breast imager using MIM software to generate regions of interest (ROI) encompassing the detected masses by UST. Mass margins were defined on the single best visualized/representative image upon a combination of sound speed and reflection image stacks to trace their contours, generating a surface area. Once tumor margins were defined, a peritumoral region was then digitally created to extend 20% of the tumor‘s diameter beyond all tumor margins, making it proportionate for every tumor. The quantitative parameters of SS and the peritumoral surface area could then be compared with the boundaries inside the traced mass ROI. The SS image was also segmented into two regions corresponding to dense and fatty tissues by using a k-means segmentation method. Combining the segmented SS image with the ROI masks allowed for calculations of the percent density (PD) [the area of dense tissue compared to the total area] for each region as well. Comparisons of mean values between the mass types were performed using an ANOVA analysis. Chi-squared test was used to assess significance of frequency differences.

3 Results

Coronal imaging by UST provided reliable circumferential evaluation of the FGI, allowing a consistent peripheral visual search pattern. Cancers were classified at the FGI in 93.3% (169/181) of the cases, were surrounded by fat in 5.5% (10/181) or parenchyma in 1.1% (2/181)(chi-squared, $p<0.001$) of cases (Figure 3). Even when surrounded by fat, cancers were still associated with residual fibrous bands (i.e., Cooper's ligaments) of the atrophied parenchyma at the FGI. For fibroadenomas, 68.6% (129/188) were classified at the FGI while 39.8% (69/173) of cysts were found at the FGI. Moreover, 56.1% (97/173) of cysts and 25.0% (47/188) of fibroadenomas were fully surrounded by dense tissue, significantly more than cancers (1.1%) (chi-squared, $p<0.001$). Few cancers, fibroadenomas or cysts were completely surrounded by fat (i.e., 5.5%, 6.4% and 4.0%, respectively).

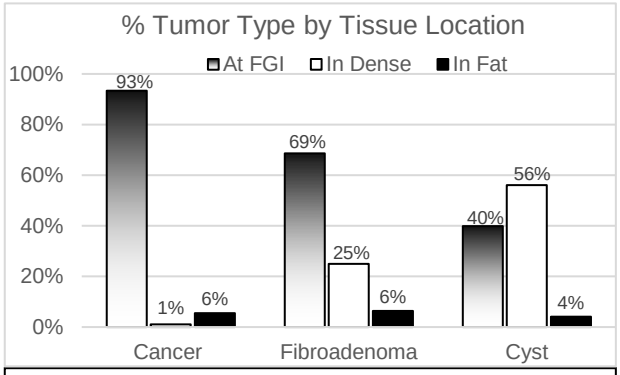

Figure 3: Relative distribution of 3 tissue locations for each tumor type (i.e., 3 locations = 100%). Significant opposing trends are noted for location incidence of Cancer, Fibroadenoma and Cyst at the FGI (shaded bars) versus being surrounded by dense breast parenchyma (white bars). A low percentage of all tumors are surrounded only by fat (black bars).

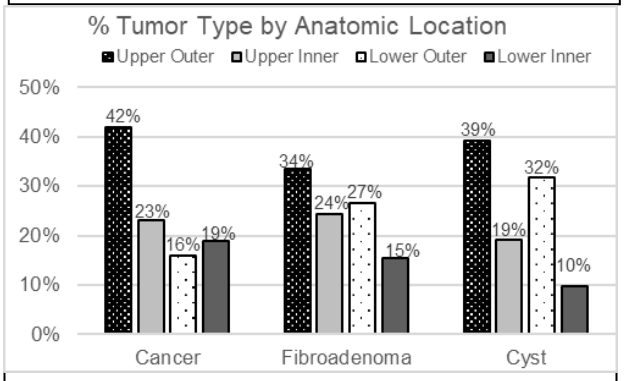

Figure 4: Relative distribution of 4 anatomic breast quadrants for each tumor type (i.e., 4 locations = 100%). All tumors were more commonly located in the upper outer quadrant and have their lowest incidence in the lower inner quadrant, but otherwise showed no mass-specific intra-quadrant differentiation.

Figure 4 shows the four-quadrant distribution of cancers, fibroadenomas and cysts. Significantly greater cancer distribution of 42% (76/181) (chi-squared, $p = 0.008$) was noted in the upper outer quadrant compared to cancer rates in the other quadrants, yet a similar greater relative percentage of 34% (63/188) for fibroadenomas and 39.3% (68/173) of cysts were also more common in the upper outer quadrant than the other locations (Chi square $p<0.01$). All tumors were also least commonly located in the lower inner quadrant ($p<0.05$).

Quantitative SS results for surface areas generated for the traced ROIs of the mass showed overlap between masses, but still a significant difference in mean SS (m/sec) for the actual mass ROIs between cancers (1527 m/s, 1521-1533 95%CI) fibroadenomas (1536 m/s, 1531-1540 95% CI) and cysts (1535 m/s, 1529-1540 95% CI)($p = 0.046$). Surrounding peritumoral regions showed significantly lower mean peritumoral SS for cancers (1477 m/s, 1470-1482 95% CI) than fibroadenomas (1496 m/s, 1490-1502 95% CI) as well as lower mean peritumoral SS for fibroadenomas than cysts (1518 m/s, 1512-1523 95% CI)(ANOVA $p<0.001$). The percent density (PD) of the peritumoral region for the different mass types also showed a progressive increase in the mean values when going from cancer to fibroadenoma to cyst (47% to 65% to 84% respectively, ANOVA $p<0.001$). Furthermore, the median peritumoral PD for cysts and cancers are 98.5% and 44.7%, quantitatively indicating that roughly half of all cysts are almost entirely surrounded by dense tissue, while significantly more fat surrounds cancers.

4 Discussion

Our results confirm the common breast imaging dictum of cancers being more common in the upper outer quadrant, but also showed a similar incidence for fibroadenomas and cysts. Similar to prior MRI findings (4,5), UST tissue localization also confirmed cancers had a very strong tendency to be located at the FGI and extend these findings by demonstrating that benign masses have a weaker tendency in that regard. Moreover, quantitative peritumoral SS characteristics of the tumor microenvironment with cancers provides insights to their greater likelihood of being partially surrounded by fat compared to benign masses and support the qualitative findings.

UST is a novel breast imaging technology being explored for its potential for improving breast cancer detection in women with dense breasts (NCT#02977247). The native coronal imaging plane by SoftVue UST may facilitate simpler qualitative detection and localization of cancers, which were much more likely to be found at the FGI (figures 1, 2). Conversely, it appears rare that cancers are entirely surrounded by fibroglandular tissues, or cysts surrounded by fat (i.e., 1.1% and 4.0%, respectively). Even though overall benign masses were significantly more likely to be surrounded by fibroglandular tissue than cancers, only cysts were predominantly surrounded by parenchyma (i.e., 56.1%). These findings are further corroborated by insights provided by the mean peritumoral analyses.

UST separation of breast parenchyma from fat by SS, using segmentation K-means segmentation techniques, have been well established and correlated with breast density by mammogram and parenchymal distribution by MR (26-36). The mean SS results for mass ROIs and peritumoral regions are better understood when we note that the mean SS for the

surrounding water bath is approximately 1500 m/s. Considering that simple cysts contain similar water-like SS or density, smaller cysts appear more often to contain thicker proteinaceous fluid or inspissated debris that can markedly elevate SS.

Data from our peritumoral analyses lend insights to the average tissue composition surrounding masses. Progressively increasing mean SS in the peritumoral tissues of cancers, fibroadenomas and cysts [i.e., 1470-1482 m/s, 1490-1502 m/s and 1512-1523 m/s respectively (ANOVA $p<0.001$)], suggest a similar physiologic progression, from a mix of fatty tissues to dense fibroglandular tissue. For cancers, the 25th percentile to 75th percentile range of mean peritumor SS is 1455 – 1499 m/s, indicating a progression of tissue composition from predominantly fatty to fairly dense, features compatible with tissues found at the FGI. Conversely, the quantitative peritumoral SS range for cysts of 1503 - 1542 m/sec is also compatible with the qualitative assessment of cysts being entirely surrounded by parenchyma a majority of the time. Using the peritumoral PD measurements also supports the qualitative analysis. The 25-75th percentile range for cancer peritumor PD goes from 14% to 75% dense, while for cysts, the same percentile range is 75% to 100% dense. Once again, this shows that the regions surrounding cancers is much more likely to be a mix of dense and fatty tissue while cysts are far more likely to be almost entirely surrounded by only dense tissue.

The preferential tumor location for cancers at, or near, the FGI thus appears to be a highly sensitive finding for cancer origin and growth, but not necessarily specific in this clinical case selection. However, the knowledge of nearly all cancers being near the FGI suggests a reasonable circumferential search pattern that will also require the use of common BI-RADS criteria. In other words, mass margin irregularity noted near the FGI is highly suspicious. Conversely, a smoothly marginated mass near the FGI still requires consideration of fibroadenoma versus more uncommon but well-marginated cancers (e.g., mucinous, medullary, etc.).

Future use as a search tool near the FGI requires comparison with an actual screening series, but the quantitative aspects of UST mass and peritumoral analyses suggest future development with computer-aided diagnosis and detection. Finally, the quantitative tumoral:peritumoral information can be further utilized to better understand the complex biology of adipocytes, adipokines and cancers cells near the FGI.

Numerous weaknesses are inherent in an analysis of a subjective criteria, such as the location of whether a breast tumor resides at the FGI. Rather than a more graded approach (4), we therefore chose a simpler assessment whereby of the extremes of being entirely surrounded by fat or fibroglandular tissue was more straightforward. While the coronal plane

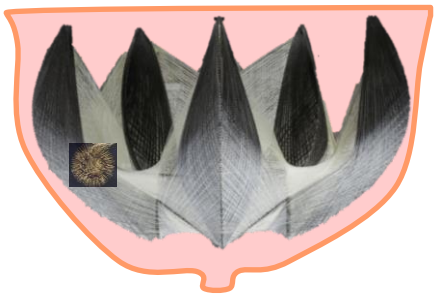

Figure 5: Graphic representation of a pendulus breast (pink background) in what could be postulated as an extremely dense breast with the FGI represented by an inverted architectural dome having a multi-pointed hemispherical mesh (black and gray). The irregularity of a cancer is represented by a burr at one of these

is convenient for the circumferential assessment of the FGI, we also acknowledge that further work is needed on the 3D assessment of both anterior and posterior tumor margins near the FGI. As a 3D structure, figure 5 is offered as a graphic rendering to show that the FGI is dispersed throughout the breast volume , but a search can be simplified to an irregularity along the FGI margin .

The FGI criteria was qualitative but produced significant mass differentiation that prior anatomic quadrant location did not. The peritumoral analyses was also incomplete for all 602 masses, being available for only 298. However, these quantitative analyses of mean SS values required no subjective component and were highly significant and supported the qualitative assessments of the FGI. Further work is also needed for further confirmation with biological and/or molecular correlates.

In summary, both the qualitative and subjective opinion of a radiologist noting cancers' preferential location at the FGI corroborates similar MR findings but emphasizes the coronal UST location as a circumferential view of the FGI. Moreover, quantitative SS results for individual masses and peritumoral regions also corroborates the well-known biological significance of fat being adjacent to cancers and their associated rate of growth. These FGI analyses showed significantly better mass differentiation than anatomic location, which confirmed that all masses are more common in the upper outer quadrant. This study supports its possible integration into clinical practice and future dense breast screening.

5 Conclusions

The coronal view by UST confirmed that cancers are much more likely to be found at the FGI ($p<0.01$) compared to fibroadenomas and cysts. UST is a novel new technology that has the potential for improved breast cancer detection. This study supports increased accuracy of UST imaging as it becomes integrated into clinical practice.

References

1. Perkins CI, Hotes J, Kohler BA, Howe HL. Association between breast cancer laterality and tumor location, United States, 1994–1998. Cancer Causes Control 2004; CCC 15:637–645.

2. Lee AH. Why is carcinoma of the breast more frequent in the upper outer quadrant? A case series based on needle core biopsy diagnoses. Breast (Edinburgh, Scotland) 2005; 14:151–152.

3. Venkatesan A, Chu P, Kerlikowske K, Sickles EA, Smith-Bindman R. Positive predictive value of specific mammographic findings according to reader and patient variables. Radiology 2009; 250(3):648-57.

4. Kim WH, Li M, Han W, Ryu HS, Moon WK. The spatial relationship of malignant and benign breast lesions with respect to the fat-gland interface on magnetic resonance imaging. Nature Sci Rep. 2016 Dec 14; 6:39085.

5. Zhu W, Harvey S, Macura KJ, Euhus DM, Artemov D. Invasive breast cancer preferably and predominantly occurs at the interface between fibroglandular and adipose tissue. Clin Breast Cancer 2017; 17(1):e11-e18.

6. Yamaguchi J, Ohtani H, Nakamura K, Shimokawa I, Kanematsu T. Prognostic impact of marginal adipose tissue invasion in ductal carcinoma of the breast. Am J Clin Pathol. 2008 Sep;130(3):382-8. doi: 10.1309/MX6KKA1UNJ1YG8VN. PMID:18701411

7. Wang YY, Attané C, Milhas D, Dirat B, Dauvillier S, Guerard A, Gilhodes J, Lazar I, Alet N, Laurent V, Le Gonidec S, Biard D, Hervé C, Bost F, Ren GS, Bono F, Escourrou G, Prentki M, Nieto L, Valet P, Muller C. Mammary adipocytes stimulate breast cancer invasion through metabolic remodeling of tumor cells. JCI Insight. 2017 Feb 23; 2(4):e87489. doi: 10.1172/jci.insight.87489. PMID:28239646.

8. Mancuso P. The role of adipokines in chronic inflammation. Immunotargets Ther. 2016; 5: 47–56.

9. Dirat B, Bochet L, Dabek M, Daviaud D, Dauvillier S, Majed B, Wang YY, Meulle A, Salles B, Le Gonidec S, Garrido I, Escourrou G, Valet P, Muller C. Cancer-associated adipocytes exhibit an activated phenotype and contribute to breast cancer invasion. Cancer Res. 2011; 71(7):2455-65.

10. Bochet L, Lehuédé C, Dauvillier S, Wang YY, Dirat B, Laurent V, Dray C, Guiet R, Maridonneau-Parini I, Le Gonidec S, Couderc B, Escourrou G, Valet P, Muller C. Adipocyte-derived fibroblasts promote tumor progression and contribute to the desmoplastic reaction in breast cancer. Cancer Res 2013; 73(18):5657-68.

11. S. Johnson, D.T. Borup, J.W. Wiskin, M. Berggren, B. Hanover, F. Setinsek, et al. From Laboratory To Clinical Trials: An Odyssey Of Ultrasound Inverse Scattering Imaging For Breast Cancer Diagnosis. *The Journal of the Acoustical Society of America*. **120**: p. 3023 (2006).

12. S.A. Johnson and M.L. Tracy ML. Inverse Scattering Solutions By a Sinc Basis, Multiple Source, Moment Method. *Part I: Theory, Ultrasonic Imaging*, **5**:361-375, (1983).

13. J.S. Schreiman, J.J. Gisvold, J.F. Greenleaf, R.C. Bahn. Ultrasound Transmission Computed Tomography Of The Breast. *Radiology*; **150**:523-30, (1984).

14. G.H. Glover. Computerized Time-Of-Flight Ultrasonic Tomography For Breast Examination. *Ultrasound In Medicine & Biology*. **3**(2-3):117-27, (1977).

15. F.A. Natterer. Propagation Backpropagation Method for Ultrasound Tomography, *Inverse problems*; **11**:1225-1232, (1995).

16. P.L. Carson, C.R. Meyer, A.L. Scherzinger, T.V. Oughton. Breast Imaging In Coronal Planes With Simultaneous Pulse Echo And Transmission Ultrasound. *Science*. **214**(4525):1141-3, (1981).

17. M. P. Andre, H.S. Janee, P. J. Martin, G. P. Otto, B. A. Spivey, D. A. Palmer, High-Speed Data Acquisition In A Diffraction Tomography System Employing Large-Scale Toroidal Arrays, *International Journal of Imaging Systems and Technology*. **8**:137-147, (1997).

18. S.A. Johnson, D. T. Borup, J.W. Wiskin, F. Natterer, F. Wuebbling, Y. Zhang, C. Olsen Apparatus and Method for Imaging with Wavefields using Inverse Scattering Techniques. United States Patent 6,005,916 (1999).

19. V.Z Marmarelis, T. Kim, R.E. Shehada, Proceedings of the SPIE: Medical Imaging 2003; San Diego, California; Feb. 23-28, 2002. Ultrasonic Imaging and Signal Processing – Paper 5035-6.

20. D.L. Liu and R. C. Waag, Propagation and backpropagation for ultrasonic wavefront design, *IEEE Trans. on Ultras. Ferro. and Freq. Contr*. **44**(1):1-13 (1997).

21. H. Gemmeke and N. Ruiter. 3D Ultrasound Computer Tomography for Medical Imaging. *Nuclear instruments and methods in Physics Research Section A: Accelerators, Spectrometers, Detectors and Associated Equipment*, **580**: 1057-1065, (2007).

22. N. Ruiter, G. Göbel, L. Berger, M. Zapf and H. Gemmeke Realization of an Optimized 3D USCT, *Proc. SPIE* **7968**, 796805 (2011)

23. N. Duric, P.J. Littrup, L. Poulo, A. Babkin, R. Pevzner, E. Holsapple, O. Rama, and C. Glide. Detection of Breast Cancer With Ultrasound Tomography: First Results with the Computed Ultrasound Risk Evaluation (CURE) Prototype. *Med Phys*. **34**: 773-85, (2007).

24. C. Li, G.S. Sandhu, M. Boone, N. Duric, P. Littrup, M. Sak, and K. Bergman. Breast Tissue Characterization with Sound Speed and Tissue Stiffness. In *Proceedings of the International Workshop on Medical Ultrasound Tomography*: 1.-3. Nov. 2017, Speyer, Germany (p. 217). KIT Scientific Publishing (2018).

25. B. Ranger, P.J. Littrup, N. Duric, P. Chandiwala-Mody, C. Li, S. Schmidt, J. Lupinacci. Breast Ultrasound Tomography versus MRI For Clinical Display of Anatomy and Tumor Rendering: Preliminary Results. *AJR Am J Roentgenol*; **198**:233-9, (2012).

26. C. Glide, N. Duric, P. Littrup: Novel Approach to Evaluating Breast Density Utilizing Ultrasound Tomography. *Med Phys*, **34**:744-753, (2007).

27. C.K. Glide-Hurst, N. Duric, P. Littrup: Volumetric breast density evaluation from ultrasound tomography images. *Med Phys* , **35**:3988-3997, (2008).

28. N. Duric, N. Boyd, P. Littrup, M. Sak, L. Myc, C. Li, E. West, S. Minkin, L. Martin, M. Yaffe, S. Schmid, M. Faiz, J. Shen, O. Melnichouk, Q. Li, and T. Albrecht. Breast Density Measurements with Ultrasound Tomography: A Comparison with Film and Digital Mammography. *Med Phys*; **40**(1): 013501, (2013).

29. N. Duric, M. Sak, S. Fan, R.M. Pfeiffer, P.J. Littrup, M.S. Simon, D.H. Gorski, H. Ali, K.S. Purrington, R.F. Brem, M.E. Sherman, G. Gierach. Using Whole Breast Ultrasound Tomography to Improve Breast Cancer Risk Assessment: A Novel Risk Factor Based on the Quantitative Tissue Property of Sound Speed. *Journal of Clinical Medicine.* **9**(2): E367. doi: 10.3390/jcm9020367, (2020).

30. Z.G. Khodr, M.A Sak, R.M. Pfeiffer, N. Duric, P. Littrup, L. Bey-Knight, H. Ali, P. Vallieres, M.E. Sherman, and G.L. Gierach. Determinants of The Reliability of

Ultrasound Tomography Sound Speed Estimates as A Surrogate for Volumetric Breast Density. *Medical Physics*; **42**(10), pp.5671-5678, (2015).

31. G.Y. Sandhu, C. Li, O. Roy, S. Schmidt and N. Duric. Frequency Domain Ultrasound Waveform Tomography: Breast Imaging Using A Ring Transducer. *Physics in Medicine & Biology*; **60**(14), p.5381 (2015).

32. M. Sak, N. Duric, P. Littrup, L. Bey-Knight, H. Ali, P. Vallieres, M.E. Sherman, and G.L. Gierach. Using Speed of Sound Imaging to Characterize Breast Density. *Ultrasound Med Biol*, **43**(1): 91-103 (2017).

33. J. Wiskin, B. Malik, R. Natesan, M. Lenox. Quantitative Assessment of Breast Density Using Transmission Ultrasound Tomography. *Med Phys*. **46**(6):2610-20, (2019).

34. E.A.M. O'Flynn, J. Fromageau, A.E. Ledger, A. Messa, A. D'Aquino, M.J. Schoemaker, M. Schmidt, N. Duric, A.J. Swerdlow, and J.C. Bamber. Ultrasound Tomography Evaluation of Breast Density: A Comparison with Non-Contrast Magnetic Resonance Imaging. *Invest Radiol* **52**(6): 343-348 (2017).

35. P.J. Littrup, N. Duric, C. Li, M. Sak, G. Sandhu, K. Bergman, et al. Current challenges in breast screening and diagnosis: From molecules to peritumoral regions and radiomics - The emerging imaging of whole breast stiffness. *Proceedings of the International Workshop on Medical Ultrasound Tomography: 1.-3., Speyer, Germany (*2017).

36. N. Duric, P. Littrup, C. Li, O. Roy, S. Schmidt, J. Seamans, A. Wallen, and L. Bey-Knight, L., 2015, March. Whole breast tissue characterization with ultrasound tomography. In *Medical Imaging: Ultrasonic Imaging and Tomography*, **9419**: 94190G (2015). International Society for Optics and Photonics.

37. E.A.M. O'Flynn, J. Fromageau, A.E. Ledger, A. Messa, A. D'Aquino, M.J. Schoemaker, M. Schmidt, N. Duric, A.J. Swerdlow, and J.C. Bamber. Ultrasound tomography evaluation of breast density: A comparison with non-contrast magnetic resonance imaging. *Invest Radiol* **52**(6): 343-348 (2017).

38. P.J. Littrup, R.A. Kane, C.R. Williams, T.K. Egglin, F. Lee, S. Torp-Pedersen, P.A. Church. Determination of prostate volume with transrectal us for cancer screening. Part I: Comparison with prostate specific antigen assays. *Radiology*; **178**:537-542 (1991).

39. P.J. Littrup, C.R. Williams, T.K. Egglin and R.A. Kane. Determination of prostate volume with transrectal us for cancer screening. Part II: The accuracy of in vitro and in vivo techniques. *Radiology* 1991; **179**:49-53 (1991).